Article

Optimization Framework for Temporal Interference Current Tibial Nerve Stimulation in Tibial Nerves Based on In-Silico Studies

Eunseon Kim [1,†], Eunbi Ye [1,†], Jiho Lee [1,†], Taekyung Kim [2,3], Dongil Choi [3,4], Kyusung Lee [3,5] and Sungmin Park [1,6,7,8,*]

1   Department of Convergence IT Engineering, Pohang University of Science and Technology (POSTECH), Pohang 37673, Republic of Korea
2   Biomedical Engineering Research Center, Samsung Medical Center, Seoul 06351, Republic of Korea
3   Department of Medical Device Management and Research, SAIHST, Sungkyunkwan University, Seoul 06351, Republic of Korea
4   Department of Radiology, Samsung Medical Center, Sungkyunkwan University School of Medicine, Seoul 06351, Republic of Korea
5   Department of Urology, Samsung Medical Center, Sungkyunkwan University School of Medicine, Seoul 06351, Republic of Korea
6   Department of Electrical Engineering, Pohang University of Science and Technology (POSTECH), Pohang 37673, Republic of Korea
7   Department of Mechanical Engineering, Pohang University of Science and Technology (POSTECH), Pohang 37673, Republic of Korea
8   Institute of Convergence Science, Yonsei University, Seoul 03722, Republic of Korea
*   Correspondence: sungminpark@postech.ac.kr
†   These authors contributed equally to this work.

Abstract: Compared to the existing noninvasive methods, temporal interference (TI) current stimulation is an emerging noninvasive neuromodulation technique that can improve the ability to focus an electrical field on a target nerve. Induced TI field distribution depends on the anatomical structure of individual neurons, and thus the electrode and current optimization to enhance the field focus must reflect these factors. The current study presents a TI field optimization framework for focusing the stimulation energy on the target tibial nerve through extensive electrical simulations, factoring in individual anatomical differences. We conducted large-scale in-silico experiments using realistic models based on magnetic resonance images of human subjects to evaluate the effectiveness of the proposed methods for tibial nerve stimulation considering overactive bladder (OAB) treatment. The electrode position and current intensity were optimized for each subject using an automated algorithm, and the field-focusing performance was evaluated based on the maximum intensity of the electric fields induced at the target nerve compared with the electric fields in the neighboring tissues. Using the proposed optimization framework, the focusing ability increased by 12% when optimizing the electrode position. When optimizing both the electrode position and current, this capability increased by 11% relative to electrode position optimization alone. These results suggest the significance of optimizing the electrode position and current intensity for focusing TI fields at the target nerve. Our electrical simulation-based TI optimization framework can be extended to enable personalized peripheral nerve stimulation therapy to modulate peripheral nerves.

Keywords: temporal interference stimulation; tibial nerve stimulation; noninvasive neurostimulation; overactive bladder syndrome; simulation based on MR image

1. Introduction

People with overactive bladder (OAB) syndrome have the symptoms of abnormally frequent urination (more than 8 times within 24 h) and nocturia which can severely decrease their quality of life [1,2]. OAB is highly prevalent and widespread with 17 million cases in the United States and 50–100 million worldwide [1]; thus, the development of effective

clinical treatments for OAB has received global attention. Conventional therapies based on medications such as antimuscarinic or anticholinergic agents remain the primary treatment options for OAB [3]. However, these methods are known to cause severe side effects such as dry mouth, blurred vision, constipation, and urine retention [4,5]. A few recent studies have reported that pharmacotherapies fail to relieve OAB symptoms in 46.2% of patients, who then decide to discontinue treatment [6,7]. To overcome the current limitations of pharmaceutical approaches, neurostimulation targeting peripheral nerves was suggested as an alternative treatment based on etiological evidence that neurological dysfunction induces OAB [8–10].

Neurostimulation modalities such as sacral nerve stimulation (SNS) using an implantable neuroprosthetic device [11], and percutaneous tibial nerve stimulation (PTNS) using invasive needle electrodes, have been clinically used for treating refractory OAB in patients experiencing pharmacotherapy side effects [11–14]. However, due to their invasive nature, they can cause significant discomfort and carry procedural risks such as the spreading of infections [15]. In this regard, transcutaneous electrical nerve stimulation (TENS) has been proposed as a noninvasive modality [16,17]. While TENS has gained considerable attention owing to the significant advantage of noninvasiveness, it is considered less effective than the invasive modalities due to its low penetration efficiency and reduced coupling of stimulation current into the body [18]. Due to this low penetration efficiency, side effects such as redness, skin burns, and pain associated with electrical stimulation have been reported after increasing the stimulation intensity during TENS [16]. Therefore, the development of a noninvasive modality with a high penetration rate is one of the most important challenges in enhancing the effectiveness of noninvasive neurostimulation methods to treat OAB [19].

Temporal interference (TI) stimulation is a recently proposed noninvasive stimulation modality that can direct stimulation energy toward tissues deep inside the body, thus avoiding off-target stimulation of shallow tissues near the skin [20]. This method uses two temporally interfering electric fields with different high carrier frequencies in the kHz range, and the difference in the carrier frequencies is small, i.e., in the range of 10's of Hz. High carrier frequencies allow the electric fields to be delivered deep inside the body due to reduced electrical impedances of tissues at such high frequencies [21], enabling their interference to form an envelope focused only in the deep region. The envelope frequency is equal to the small frequency difference of less than 40 Hz [20], which is low enough to stimulate the target nerves; however, the frequencies are rather high in the kHz range, causing no response from the nerves [22]. On comparing the existing noninvasive stimulation techniques in regard to this property, TI stimulation requires a low current intensity to stimulate the nerves deep inside the body due to high penetration efficiency, thereby preventing adverse effects of superficial tissue injuries near the skin surface [23]. Considering these advantages, in our previous study, we proposed and demonstrated the feasibility of TI stimulation for OAB treatment using both an in-silico human model and an in-vivo rat model [18]. However, the study had the limitation of the small number of human models, similar to that in other in-silico studies using less than 10 models [18,23–28]. This is an insufficient number of models to evaluate the clinical applicability of TI stimulation, considering individual anatomical differences. Therefore, a large-scale in-silico study using realistic human models is required to provide robust preclinical evidence for the clinical application of TI stimulation [29,30].

The main goals of this study were to confirm the effectiveness of TI stimulation as an alternative OAB-treating neuromodulation technique through a large-scale in-silico study and develop an optimization technique to focus TI fields on the tibial nerve. To achieve these goals, we developed additional human leg models based on clinical MR images and suggested a framework to optimize input currents and placements of electrodes to maximize the localization of induced electric fields in the target tibial nerve for OAB treatment through electrical stimulation. The focusing was controlled by automatically changing the placement of electrodes or by altering the current intensity for each electrode [20,23].

The remainder of this paper is organized as follows. Section 2 presents the MR data acquisition and modeling process, as well as the stimulation conditions and post-processing for TI optimization verification. In addition, this section introduces formulas for implementing TI stimulation and describes indexes for evaluating targeting ability. Section 3 presents the results, and Section 4 suggests their interpretation. Section 5 concludes our study.

2. Materials and Methods

The focusing ability was quantified with the field intensity at the tibial nerve relative to the non-target region and evaluated through large-scale in-silico experiments using several human models based on the subjects' magnetic resonance (MR) imaging data. The imaging-based realistic models enabled the analysis of the effects of individual anatomical differences in tissue distribution. Figure 1 illustrates the overall optimization procedure of TI stimulation and the application of TI stimulation in the lower leg model where the target region exists. The left side of Figure 1a shows an example of the location of the tibial nerve as the target area in the human phantom model. The right side of Figure 1a presents the result of a 3D model constructed using the acquired MR data. The concept of TI stimulation applied to the lower leg model is illustrated in Figure 1b. Enhanced energy transfer in nerve regions different from that realized using a single electric field is observed.
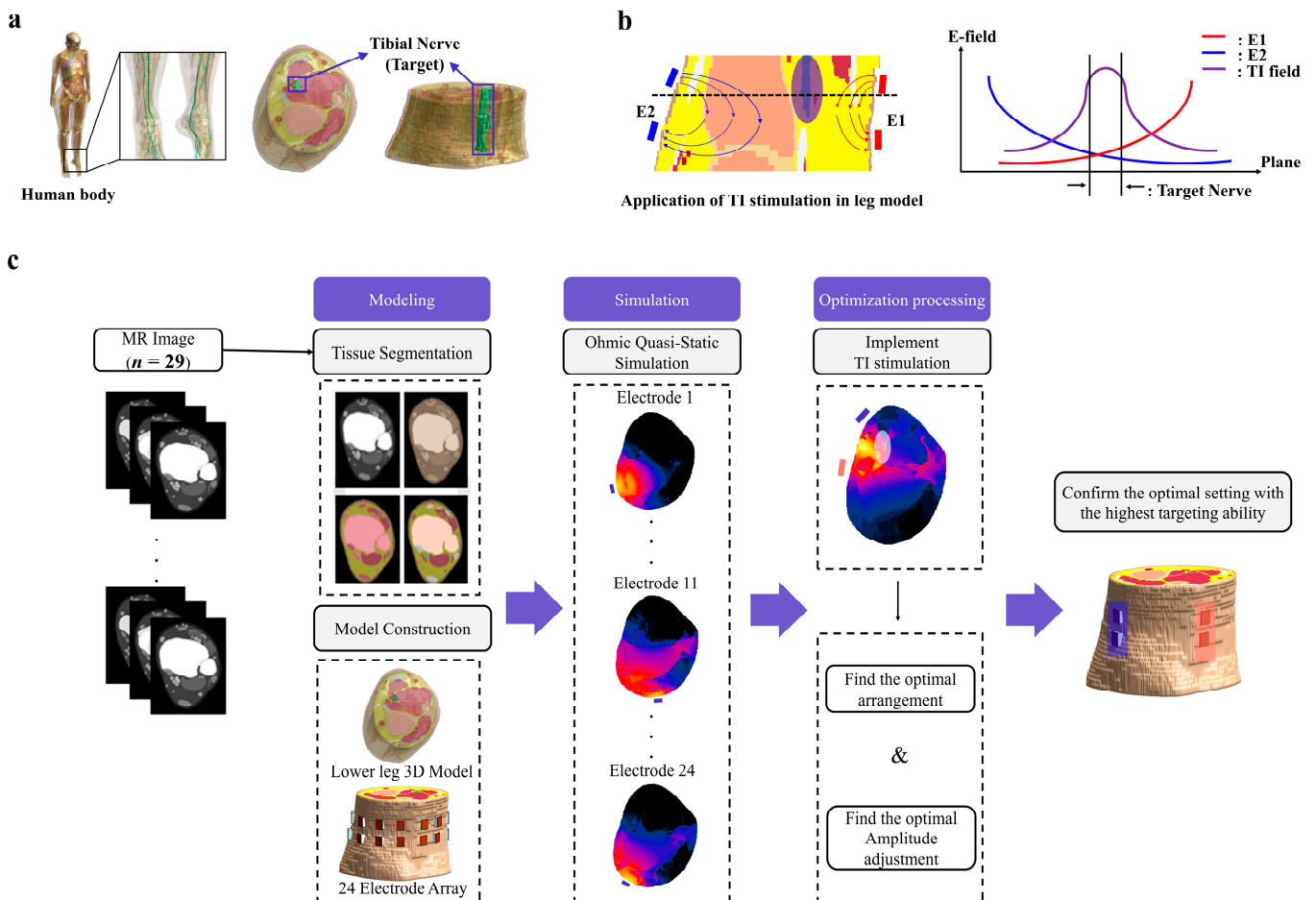

Figure 1. Concept of TI current stimulation on the tibial nerve and optimization of the TI stimulation framework. (**a**) Position of the target area (tibial nerve) in the human phantom model (left) and the target area in the MR-based 3D model (right). (**b**) Concept of applying TI stimulation to the peripheral region. (**c**) Overall processing for TI stimulation optimization.

The optimization process is shown in Figure 1c. After constructing a 3D model using the MR imaging data of 29 people, 24-array electrodes were placed. Formation of the

individual electric fields is achieved when selecting the stimulation parameters for each electrode. Optimization algorithms determine the optimal electrode pair conditions and current ratios of the electric field for all electrodes in post-processing. This procedure was repeated for all models.

2.1. MR Datasets

For a 3D model generation, we collected a set of MR images of an ankle from subjects who had T1- and T2-weighted axial images for clinical purposes. The magnetic resonance imaging (MRI) examinations were performed on 3.0 T MRI scanners (Ingenia 3.0T; Philips Healthcare, Amsterdam, The Netherlands), and a set of images was extracted from the top of the MRI to the end of the medial malleolus with a slice thickness of 2 mm. As a result, 15–30 slices covering 3–6 cm proximal to the tip of the medial malleolus were included for each subject. All MRI data were reviewed by a radiologist, and only subjects whose images were clinically normal were included in the dataset. Finally, MR images of 29 subjects were used in this study. The characteristics of the subjects are shown in Table 1. After the dataset was established, the tissues in each slice image were classified by the radiologist into 8 different types.

Table 1. Subjects' characteristics.

Characteristics	Value
Number of subjects	29
Age (Years)	42.3 ± 15.9 (19–76)
Gender (Male:Female)	13 (44.83%):16 (55.17%)
Ankle direction (Right:Left)	18 (62.07%):11 (37.93%)

This study was approved by the Institutional Review Board of the Samsung Medical Center and was carried out according to the Declaration of Helsinki. Because we used existing data collected for clinical purposes, the need for informed consent was waived. Additionally, the dataset was anonymized to protect the identity of the individual patient.

2.2. 3D Modeling Using MR Images

Figure 2 shows the process of constructing an individual 3D leg model from the subject's MR images and the composition of assigned tissues in the model. Figure 2a shows the modeling process using acquired MR images. Tissue segmentation was performed using the iSeg program (ZMT Zurich medTech AG, Zurich, Switzerland) on individual raw MR images. For each segmented data, a 3D model was constructed by the process of stacking slices using Sim4Life (ZMT Zurich medTech AG). The completed 3D model and cross-section for checking the anatomical differences are shown in Figure 2a (right). The 3D modeling results for all data and cross-sectional views of the 29 models are shown in Figure S1. Anatomical differences can be identified from the cross-sectional views of the 29 models. Tissues were classified into 8 types: skin, fat, muscle, tendon ligament, blood vessel, nerve, bone, and bone marrow, as shown in Figure 2c.

Virtual electrodes were placed on the model for TI stimulation. Each electrode had dimensions of 7 mm (width) × 7 mm (length) × 0.5 mm (height). The conductive gel featured the same width and length as the electrode; however, the thickness ranged from 0.5 to 5 mm due to the unevenness of the skin surface. The conductivity of each tissue and gel is indicated in Table 2, and the IT'IS LF 4.0 standard was used for living tissue. This standard is provided by the IT IS Foundation and indicates the electrical conductivity for frequencies up to 1 MHz for all tissues, based on a combination of the Gabriel dispersion relations and the values from other available literature [31]. The conductivity of the gel was specified as 0.6 S/m [18].
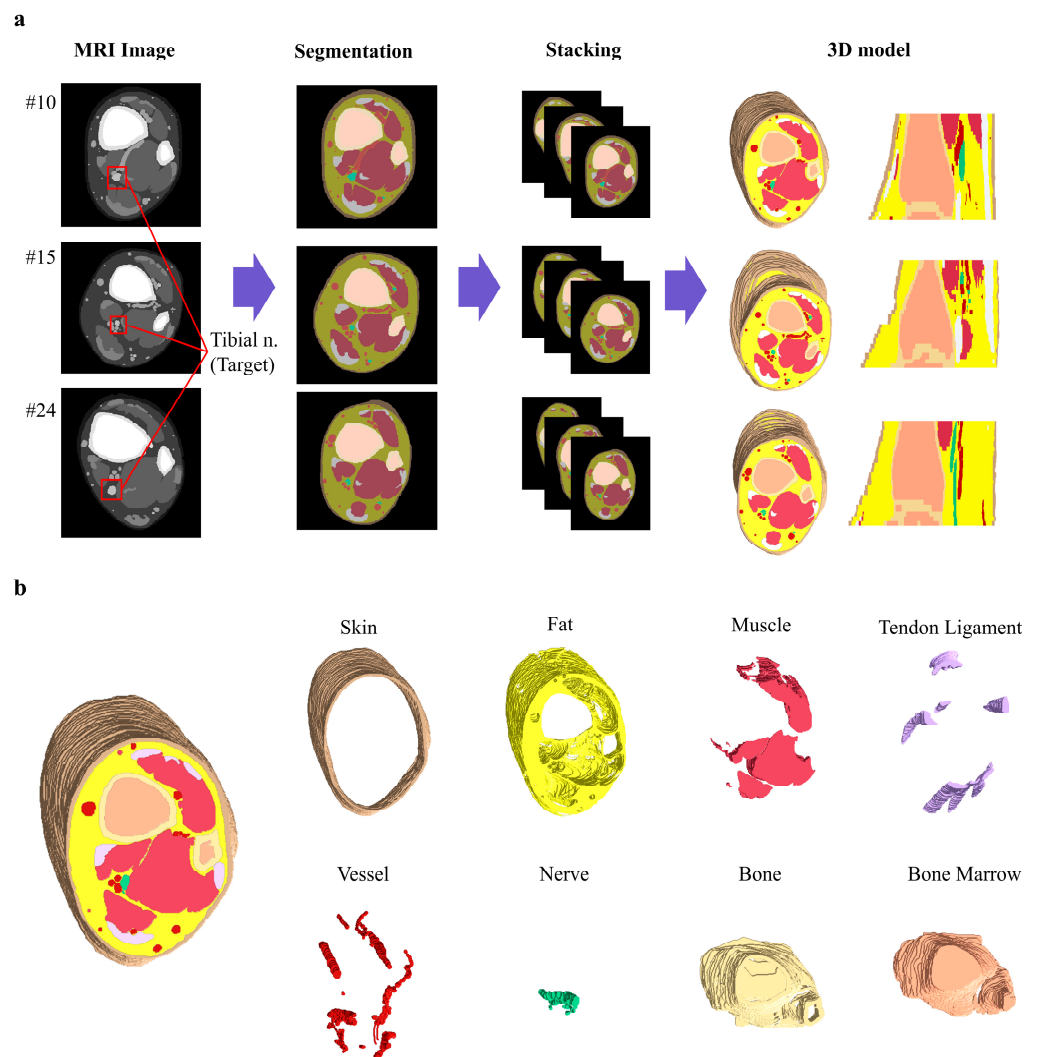
Figure 2. Models based on MR data (*n* = 29) and tissue composition. (**a**) Construction process of a 3D lower leg model based on MR data. (**b**) Tissue composition in the construction model. For visibility, the tendon ligament has been colored purple only in that figure.

Table 2. Conductivity of each material included in the optimization.

Material	Conductivity σ (S/m)
Skin	0.17
Fat	0.0573412
Muscle	0.355287
Tendon Ligament	0.367577
Vessel	0.231972
Nerve	0.265076
Bone	0.00350399
Bone Marrow	0.00247168
Gel	0.6

2.3. Simulation of Independent Electric Field Formation

Since independent electric field formation for each electrode is required to find the electrode pair for optimal field distribution, we placed an additional reference electrode [23]. The reference electrode was placed on the medial malleolus in all models.

In 24 separate simulation settings corresponding to each electrode, Dirichlet boundary conditions of 1 V for the active electrode and 0 V for the reference electrode were imposed.

The injection current of the active electrode was subsequently scaled to 1 mA for all simulations. All simulations were conducted using Sim4Life (ZMT Zurich medTech AG). Since the electrode was implemented using gel, the Ohmic Quasi-Static method was used as the finite element method to investigate the Ohmic conductive effect. Post-processing was performed on all 24 cases by repeating this process, and the electric field distribution of each of the 29 subjects was evaluated.

2.4. Post-Processing to Identify Optimal Conditions

Based on the results of each of the 24 independent simulations, we investigated the optimal conditions through TI stimulation implementation. First, we selected two pairs of electrodes for individual electric field formation. The electrode pair consisted of an active electrode and a reference electrode. The active electrodes of each pair were selected at a different height of the row. When two electric fields formed through an electrode pair are superpositioned through field subtraction, no current flows through the reference electrode. This process was repeated to form independent electric fields, E1 and E2.

Subsequently, we used the following formula to implement the TI stimulation:

$$E_{total} = ||E_1 + E_2| - |E_1 - E_2|| \tag{1}$$

This was calculated for all possible electrode combinations, and the optimal electrode setting was determined using the peak ratio (PR) value as an index to consider targeting ability and energy transfer efficiency [32,33].

$$\text{PR} = \frac{E_{target}}{E_{total}} \tag{2}$$

E_{target} is the average value of the E-field in the nerve area, and the E_{target} of the individual target area was calculated by calculating the coordinate values considering the position and size of the subject's nerve. E_{total} is the average value of the E-field of the entire area including the target area. To minimize numerical error, the PR value was calculated using the average value, rather than the maximum value used in the previous formula. By adjusting the electrode positions and current intensities, which we suggested as optimization factors, we determined that the highest PR value condition was the optimal condition. A post-processing algorithm to automatically determine optimal parameter settings was written using MATLAB R2020b. This algorithm calculated the PR values for all possible electrode pair combinations, which then resulted in the highest PR value condition. This post-processing was performed on all subjects.

3. Results

3.1. Necessity of TI Stimulation Optimization

Figure 3 suggests the importance of optimizing the TI stimulation parameters. We arranged 24 electrodes in two rows as shown in Figure 3a and numbered the electrodes in the counterclockwise direction according to the position of the reference electrode. To understand the electrode arrangement, the slices of the 1st layer and 2nd layer are displayed on the right side of Figure 3a. In the 1st layer, the electrode at the same position as the reference electrode is designated as No. 1, and the number of electrodes in all layers is 12. Electrodes numbered 13 to 24 are present in the 2nd layer. The reference electrodes are placed for individual E-field formation.

In this section, electrode pairs are formed with electrodes in the same position on the first and second layers. Since the two electrode pairs that form the electric fields E1 and E2 are in a parallel relationship, this was named a parallel electrode pair. All models were evaluated for the lowest and highest PR values in the case where only parallel electrode pairs were allowed. Figure 3b shows the concept for all parallel electrode pair evaluations. The red and blue dots indicate the positions of the electrode pairs, and it can be confirmed that the electrode pairs do not cross and have a parallel relationship. The purple dot

indicates the area where energy is concentrated when TI stimulation is applied using the two electrode pairs. The focused area changed depending on the location of the electrode, and the conditions of the electrode location where energy was concentrated in the target area were investigated.
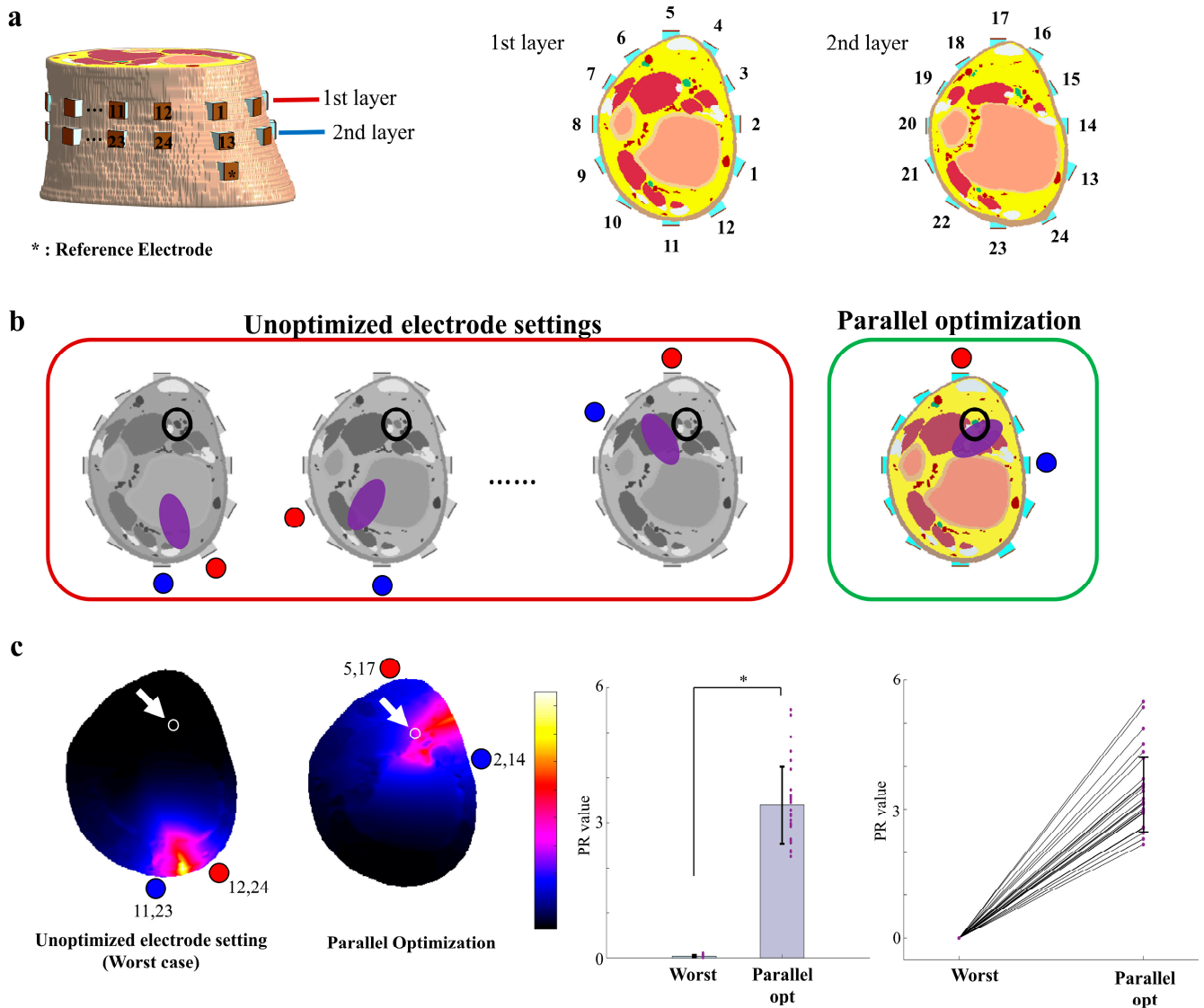

Figure 3. Comparison of TI stimulation results in the worst case and parallel electrode pair optimization. (**a**) Example of an electrode arrangement for TI stimulation (**b**) Concept of an unoptimized electrode setting and optimized electrode setting. (**c**) Comparison of worst TI and parallel opt TI results, * $p < 0.001$.

The left side of Figure 3c compares the E-field slice distribution results of the worst-case and parallel optimizations. The setting that was optimized for parallel pairs was called parallel optimization TI. The right side of Figure 3c shows the comparison of the difference in PR values of the worst TI and parallel opt TI for all models. To visualize the difference between the PR values of the two groups, the PR value of the worst TI for each subject was set at 0, the reference point, and the difference between the PR values of the parallel opt TI and worst TI is displayed on the right side. For the worst TI, the PR value was 0.0389 ± 0.0231 (mean $\pm$ standard deviation). For the parallel opt TI, the PR value was 3.3957 ± 0.8553. E_{total} was the average value of the electric fields in the entire area, including areas not activated by stimulation, whereas E_{target} was the average of electric fields induced in the only target nerve. We calculated the ratio of the average value of the

electric field of the entire area and the target area as the PR value to prevent numerical errors. As the targeting ability improves, the energy is concentrated in the targeted area while minimizing the energy in the unwanted background area. Therefore, the average value of the energy in the target area is much higher than the average value of the energy in the entire background area, which may result in higher PR values than in studies using previous PR values.

To confirm the significance of the average difference in PR values, a paired *t*-test was performed. Purple dots represent raw data. The mean and standard deviation of the changes are shown in black. The PR value of the parallel opt TI was 87 times higher than that of the worst TI ($p < 0.001$).

3.2. Improvement of TI Stimulation Optimization with Free Pair Acceptance of Electrodes

Electrodes were randomly chosen to validate the optimization of electrode pair combinations for the two most crucial factors in TI stimulation: (1) electrode pair combination and (2) difference in current adjustment. More electrode combinations were calculated by allowing a free selection of electrodes instead of selecting only parallel pairs. Accordingly, a combination of electrode pairs was made by selecting four possible electrodes, hence the total number of electrodes that could be selected was $_{24}C_4$ = 10,626 electrodes. This is referred to as cross-optimization TI (Cross opt TI). Figure 4a shows the difference in electrode arrangement between parallel opt TI and cross opt TI.
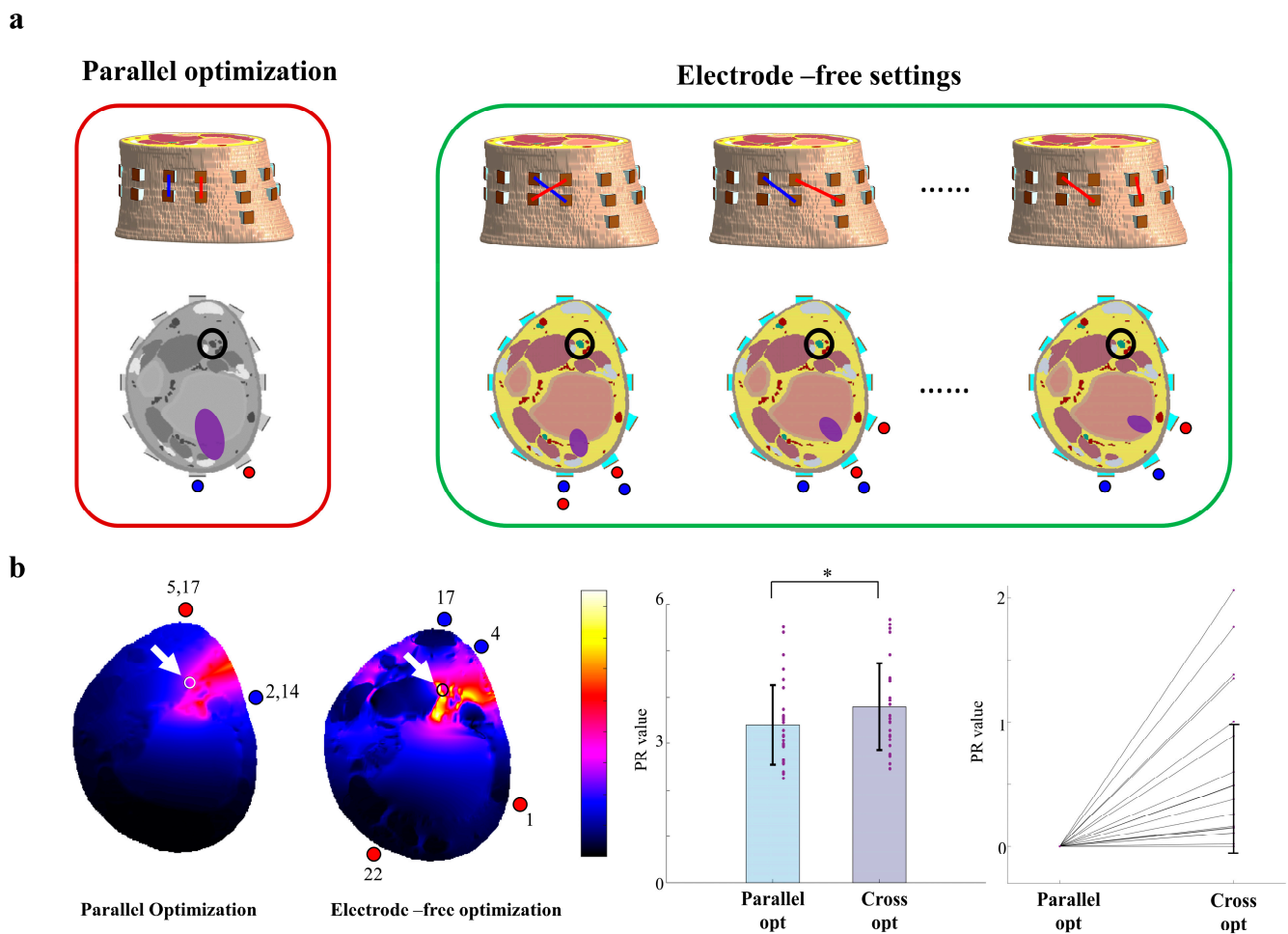

Figure 4. Comparison of TI stimulation results in parallel optimization and electrode-free optimization (**a**) Concept of electrode arrangement between parallel optimization and electrode-free settings. (**b**) Comparison of parallel opt TI and cross opt TI results, * $p < 0.005$.

The left of Figure 4b shows the slice distribution result of parallel optimization and electrode-free optimization. The right of Figure 4b shows the comparison of PR values of parallel optimization and electrode-free optimization and the difference in the PR values. For visualization purposes, the PR value of parallel opt TI for each subject was assigned to be 0 as the reference point, and the difference between the PR values of parallel opt TI and cross opt TI is displayed on the right side. As noted in the previous section, for the parallel opt TI, the PR value was 3.3957 ± 0.8553, and for Cross opt TI, the PR value was 3.7876 ± 0.9307. To confirm the significance of the average difference in PR values, a paired *t*-test was performed. The purple dots represent raw data. The mean and standard deviation of the changes are shown in black. The mean PR value of Cross opt TI was higher than that of parallel opt TI (+12%) ($p < 0.005$).

Table 3 shows a comparison of optimal electrode pairings for parallel-opt TI and cross-opt TI across all models. Subject ID refers to the ID of the patient used in the experiment. Parallel opt TI Pair refers to the optimal pair of two electrodes obtained through simulation for the patient. Since electrode pairs form an electric field, and in this methodology, they form two electric fields, so we named them E1 and E2 in descending order according to the number of electrode pairs that make up each. In all E1 and E2, the electrodes shown on the front are positively charged, and the electrodes shown on the back are negatively charged. In certain models, cross-opt TI and parallel-opt TI showed the same optimal pair conditions, but for others, the electrode settings were changed. An analysis of the corresponding anatomical factors can be seen in Figure S2.

Table 3. Electrode pair differences between parallel opt and cross opt-in all models.

Subject ID	Parallel Opt TI Pair		Cross Opt TI Pair	
0A7CE3A9878D	E1: 2, 14	E2: 4, 16	E1: 1, 19	E2: 3, 16
0BB634E25B39	E1: 2, 14	E2: 5, 17	E1: 2, 14	E2: 5, 17
0C2CD6A715D9	E1: 3, 15	E2: 5, 17	E1: 3, 15	E2: 5, 17
0C6B9FB295F5	E1: 9, 21	E2: 12, 24	E1: 9, 21	E2: 12, 24
04FD92123E3B	E1: 1, 13	E2: 6, 18	E1: 5, 16	E2: 10, 13
049DE0BA46DB	E1: 2, 14	E2: 4, 16	E1: 2, 14	E2: 4, 16
056BB93171A1	E1: 2, 14	E2: 4, 16	E1: 1, 20	E2: 4, 15
142F50561C17	E1: 2, 14	E2: 5, 17	E1: 1, 22	E2: 4, 17
145A6B872F35	E1: 2, 14	E2: 7, 19	E1: 2, 14	E2: 7, 19
1047A2F46867	E1: 2, 14	E2: 4, 16	E1: 2, 14	E2: 4, 16
1ADD8CA28477	E1: 10, 22	E2: 12, 24	E1: 6, 14	E2: 11, 22
2C6D63044761	E1: 2, 14	E2: 4, 16	E1: 2, 19	E2: 4, 15
122A1B6D95A9	E1: 1, 13	E2: 10, 22	E1: 1, 13	E2: 10, 22
314FCC7AC93	E1: 9, 21	E2: 12, 24	E1: 9, 21	E2: 12, 24
4822C489EC4B	E1: 1, 13	E2: 5, 17	E1: 1, 13	E2: 5, 17
A7EAB9020A9B	E1: 2, 14	E2: 4, 16	E1: 2, 14	E2: 4, 16
F3DA08325EFB	E1: 11, 23	E2: 12, 24	E1: 7, 24	E2: 10, 23
FC4D5480D29B	E1: 10, 22	E2: 11, 23	E1: 9, 21	E2: 11, 13
32A8962F076D	E1: 9, 21	E2: 12, 24	E1: 9, 21	E2: 12, 24
32D584F66995	E1: 2, 14	E2: 6, 18	E1: 2, 24	E2: 4, 17
82CA5FFFD969	E1: 1, 13	E2: 11, 23	E1: 1, 20	E2: 12, 23
84F96B24DC37	E1: 9, 21	E2: 12, 24	E1: 1, 14	E2: 10, 21
86E655D35063	E1: 11, 23	E2: 12, 24	E1: 11, 21	E2: 12, 24
377F6827B403	E1: 2, 14	E2: 3, 15	E1: 2, 14	E2: 3, 15
714C5CA7D5C9	E1: 3, 15	E2: 4, 16	E1: 2, 15	E2: 4, 16
4854E61F9C73	E1: 10, 22	E2: 12, 24	E1: 6, 13	E2: 10, 23
AFA8C6F48087	E1: 10, 22	E2: 12, 24	E1: 5, 13	E2: 10, 23
BDBD4C7F4443	E1: 11, 23	E2: 12, 24	E1: 10, 24	E2: 10, 23
EB27F9C7CA47	E1: 1, 13	E2: 8, 20	E1: 10, 21	E2: 12, 24

3.3. Comparison of Improvements in Maximum Optimization

We then compared cross-opt TI with the final optimization TI method, where we applied both current adjustment and the free selection of electrode pairs (Intensity opt TI). Figure 5a shows cross-opt TI and the current adjustment concept for cross-opt settings, which was exclusively created for a conceptual understanding. For determining the intensity opt TI parameters, the most optimal settings were obtained by investigating all possible electrode combinations and variable current values fed to the electrodes. The current of each electric field was adjusted by 0.1 mA while the sum of the total currents of E1 and E2 was kept at 2 mA. The final optimization parameters of Intensity opt TI for all subjects are shown in Table 4.

The left of Figure 5b shows the result of the E-field cross-sectional distribution of cross-opt TI and intensity opt TI. The right of Figure 5b shows the comparison between the difference in PR values of cross-opt TI and intensity opt TI for all models. For visualization purposes, the PR value of cross-opt TI was assigned to be 0 as the reference point, for all subjects. The difference between the PR values of cross-opt TI and parallel-opt TI is shown on the right. Compared with the PR value of 3.7876 ± 0.9307 for cross-opt TI in the previous section, the PR value of intensity opt TI here was 4.2061 ± 1.1338. To confirm the significance of the average difference in PR values, a paired *t*-test was performed. Purple dots represent raw data. The mean and standard deviation of the changes are shown in black. The average PR value of Intensity opt TI was higher than that of Cross opt TI (+11%) ($p < 0.001$).
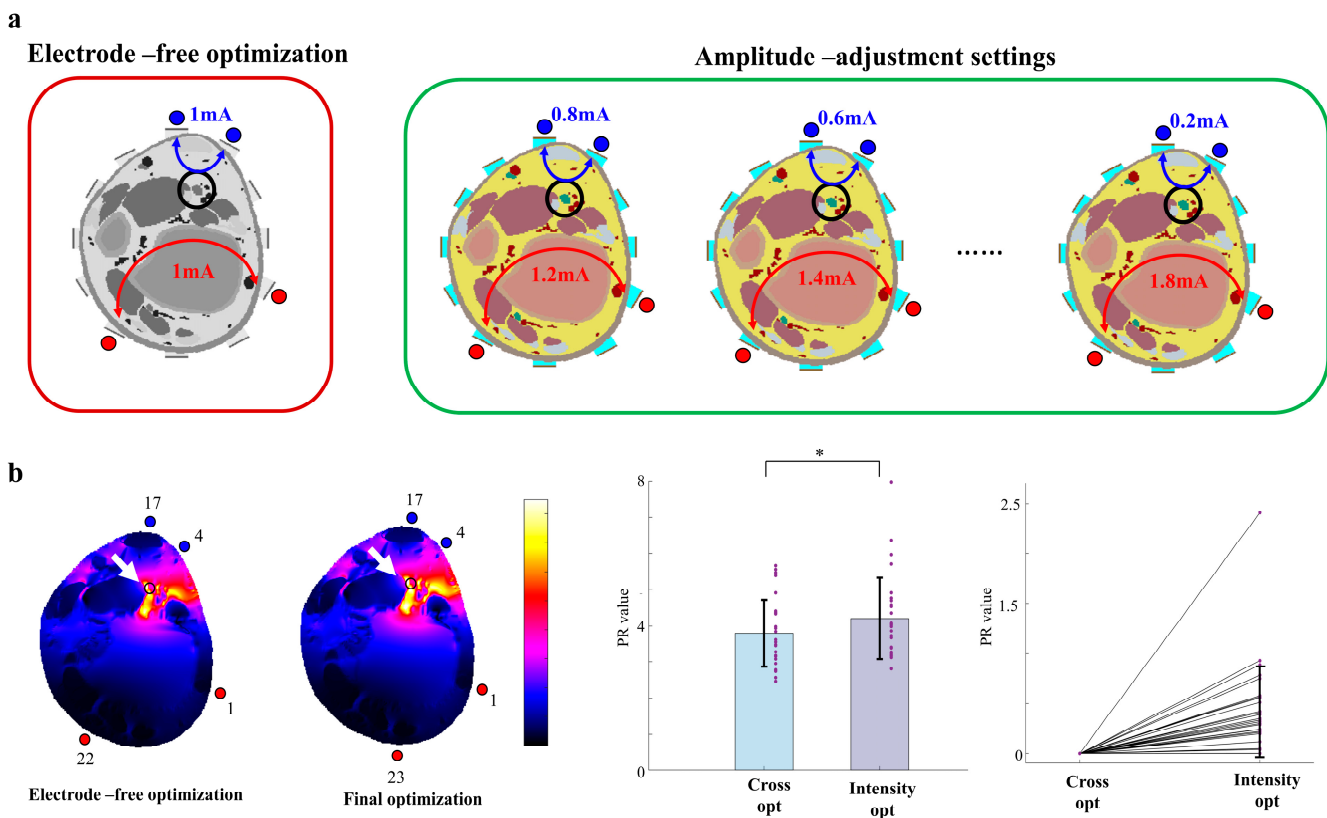

Figure 5. Comparison of TI stimulation results in electrode-free optimization and final optimization. (**a**) Concept of electrode-free optimization and amplitude-adjustment settings. (**b**) Comparison of cross opt TI and intensity opt TI results, * $p < 0.0001$.

Table 4. Optimization parameter settings for intensity opt TI.

Subject ID	Electrode Pair		Current Adjustment	
0A7CE3A9878D	E1: 3, 16	E2: 10, 19	E1: 0.6	E2: 1.4
0BB634E25B39	E1: 2, 14	E2: 4, 16	E1: 1.5	E2: 0.5
0C2CD6A715D9	E1: 3, 15	E2: 5, 17	E1: 0.9	E2: 1.1
0C6B9FB295F5	E1: 9, 21	E2: 12, 24	E1: 1.0	E2: 1.0
04FD92123E3B	E1: 2, 14	E2: 6, 18	E1: 0.5	E2: 1.5
049DE0BA46DB	E1: 2, 14	E2: 5, 17	E1: 0.8	E2: 1.2
056BB93171A1	E1: 2, 14	E2: 5, 17	E1: 0.7	E2: 1.3
142F50561C17	E1: 1, 23	E2: 4, 17	E1: 1.1	E2: 0.9
145A6B872F35	E1: 2, 14	E2: 7, 19	E1: 1.0	E2: 1.0
1047A2F46867	E1: 2, 14	E2: 5, 17	E1: 0.7	E2: 1.3
1ADD8CA28477	E1: 11, 23	E2: 12, 24	E1: 0.5	E2: 1.5
2C6D63044761	E1: 1, 19	E2: 3, 16	E1: 1.5	E2: 0.5
122A1B6D95A9	E1: 1, 13	E2: 10, 22	E1: 0.7	E2: 1.3
314FCC7AC93	E1: 9, 21	E2: 12, 24	E1: 1.1	E2: 0.9
4822C489EC4B	E1: 1, 13	E2: 4, 16	E1: 1.3	E2: 0.7
A7EAB9020A9B	E1: 1, 13	E2: 4, 16	E1: 1.5	E2: 0.5
F3DA08325EFB	E1: 1, 24	E2: 10, 23	E1: 1.4	E2: 0.6
FC4D5480D29B	E1: 9, 21	E2: 11, 23	E1: 1.4	E2: 0.6
32A8962F076D	E1: 9, 21	E2: 12, 24	E1: 1.2	E2: 0.8
32D584F66995	E1: 3, 15	E2: 6, 18	E1: 0.5	E2: 1.5
82CA5FFFD969	E1: 1, 13	E2: 11, 23	E1: 1.2	E2: 0.8
84F96B24DC37	E1: 9, 21	E2: 12, 24	E1: 1.4	E2: 0.6
86E655D35063	E1: 11, 23	E2: 12, 24	E1: 0.5	E2: 1.5
377F6827B403	E1: 1, 13	E2: 3, 15	E1: 1.5	E2: 0.5
714C5CA7D5C9	E1: 2, 14	E2: 4, 16	E1: 1.5	E2: 0.5
4854E61F9C73	E1: 7, 18	E2: 10, 23	E1: 1.4	E2: 0.6
AFA8C6F48087	E1: 10, 22	E2: 12, 24	E1: 1.2	E2: 0.8
BDBD4C7F4443	E1: 3, 13	E2: 10, 23	E1: 1.3	E2: 0.7
EB27F9C7CA47	E1: 10, 21	E2: 12, 24	E1: 0.9	E2: 1.1

4. Discussion

TI stimulation has emerged as an effective noninvasive electrical stimulation modality for modulating brain tissues. Nonetheless, its application has recently extended to the peripheral nervous system in which the surrounding tissue composition is anatomically much simpler than that of the brain. Also, there is no low conductive tissue, such as the skull in the vicinity; thus, current penetration to the deeper-lying tissues, such as nerves, is more efficient. In this regard, TI current-based tibial nerve stimulation has been recently proposed, but its applicability was evaluated via limited in-silico studies with a small number of human models; thus, the anatomical differences in individuals have yet to be attempted. Therefore, through a large-scale in-silico study using MR image-driven human leg phantoms, we evaluated the effectiveness of TI current-based tibial nerve stimulation as an OAB-treating neuromodulation technique and develop the TI field optimization framework that can overcome the individual anatomical differences to focus the induced fields on the tibial nerve.

TI stimulation requires two pairs of electrodes, and input currents and physical placement of the electrodes can largely affect the induced field distribution. Therefore, an optimal arrangement of those parameters, such as currents and placement of electrodes, is critical to overcoming the individual anatomical differences, and we developed a framework to determine the optimal stimulation condition using the individual phantom models driven from the MR images. As shown in Figure 3, the optimized placement of parallel pairs of electrodes resulted in 87 times higher PR value than the worst placement of parallel

electrodes, indicating that the field targeting ability significantly depends on the position of the electrode pair. Thus, as suggested by previous studies, optimizing the position of the electrodes when performing TI stimulation on the tibial nerve is important [18,20,23].

In the case of cross-opt TI, not only parallel pairs of electrodes but also random pairs are allowed. With such a method allowing for random selection of electrode pairs, improved targeting capability can be expected due to the greater number of possible electrode combinations. Comparisons of parallel opt TI and cross opt TI revealed the PR value of cross opt TI was higher than that of parallel opt TI. Thus, when an arbitrary electrode pair selection is allowed and the optimization algorithm is applied, a higher targeting ability is realized compared to when only a parallel pair combination is applied.

Intensity opt TI is the setting with the highest targeting ability when both the electrode position adjustment and current adjustment are considered. Comparing the Cross opt TI method with the Intensity opt TI method, the PR value of Intensity opt TI was higher. Our results suggest that current adjustment is also a significant factor in enhancing the targeting ability in the optimization of TI stimulation. Furthermore, we found that both the electrode position and current intensity must be considered when manually optimizing TI stimulation focusing. Therefore, an optimization approach using both the free selection of electrode pairs and current adjustment proved to be the most effective method.

In addition, we analyzed the anatomical factors that must be considered when performing TI optimization. Models with a small ratio of nerve depth to the total model section length showed enhanced optimization effects upon changing the optimal electrode pair settings in the Cross opt method. This implies that for clinical applications of TI stimulation, random optimization of the electrodes may be more effective for certain patients, depending on their specific anatomical characteristics. However, the exploration of parameters related to current adjustment must be confirmed through follow-up studies. These results should be utilized to provide criteria for determining the method of TI optimization.

Furthermore, we found individual optimization parameters in all models through the development of an automated TI optimization algorithm. Our results from large-scale in-silico experiments demonstrated that focusing electric fields in TI stimulation to tibial nerves using imaging-based models can provide personalized stimulation parameters for OAB treatment. This suggests that our proposed optimization framework can be easily applied to clinical practice in the future.

5. Conclusions

This study presents a TI field optimization framework to maximize the localization of the induced fields on the tibial nerve, which can enhance the effectiveness and safety of the TI stimulation while overcoming individual anatomical differences. This framework uses the individual leg phantom developed from the individual's MR image and determines the input currents and placement of two pairs of electrodes. The simulated results show that, unlike random electrode selection, an optimization process is essential for effective and safe TI stimulation for the tibial nerve. It is important to note that the findings in this study provide an essential suggestion not only for the effective treatment of OAB but also for other neurological disorders that require noninvasive peripheral nerve stimulation therapies.

Institutional Review Board Statement: This study was approved by the Institutional Review Board of the Samsung Medical Center and carried out according to the Declaration of Helsinki.

Informed Consent Statement: Informed consent was obtained from all individual participants included in the study. All authors have approved the content for publication.

Data Availability Statement: Not applicable.

Conflicts of Interest: The authors declare no conflict of interest.

References

1. Nitti, V.W. Clinical impact of overactive bladder. *Rev. Urol.* **2002**, *4*, S2.
2. Haylen, B.T.; De Ridder, D.; Freeman, R.M.; Swift, S.E.; Berghmans, B.; Lee, J.; Monga, A.; Petri, E.; Rizk, D.E.; Sand, P.K. An International Urogynecological Association (IUGA)/International Continence Society (ICS) joint report on the terminology for female pelvic floor dysfunction. *Neurourol. Urodyn. Off. J. Int. Cont. Soc.* **2010**, *29*, 4–20. [CrossRef] [PubMed]
3. Andersson, K.-E.; Yoshida, M. Antimuscarinics and the overactive detrusor—Which is the main mechanism of action? *Eur. Urol.* **2003**, *43*, 1–5. [CrossRef] [PubMed]
4. Nabi, G.; Cody, J.D.; Ellis, G.; Hay-Smith, J.; Herbison, G.P. Anticholinergic drugs versus placebo for overactive bladder syndrome in adults. *Cochrane Database Syst. Rev.* **2006**, *4*, CD003781. [CrossRef]
5. Chapple, C.R.; Khullar, V.; Gabriel, Z.; Muston, D.; Bitoun, C.E.; Weinstein, D. The effects of antimuscarinic treatments in overactive bladder: An update of a systematic review and meta-analysis. *Eur. Urol.* **2008**, *54*, 543–562. [CrossRef] [PubMed]
6. Shah, S.; Nitti, V.W. Defining efficacy in the treatment of overactive bladder syndrome. *Rev. Urol.* **2009**, *11*, 196. [PubMed]
7. Benner, J.S.; Nichol, M.B.; Rovner, E.S.; Jumadilova, Z.; Alvir, J.; Hussein, M.; Fanning, K.; Trocio, J.N.; Brubaker, L. Patient-reported reasons for discontinuing overactive bladder medication. *BJU Int.* **2010**, *105*, 1276–1282. [CrossRef]
8. Kurpad, R.; Kennelly, M.J. The Evaluation and Management of Refractory Neurogenic Overactive Bladder. *Curr. Urol. Rep.* **2014**, *15*, 1–7. [CrossRef] [PubMed]
9. Qin, C.; Wang, Y.H.; Gao, Y.L. Overactive Bladder Symptoms within Nervous System: A Focus on Etiology. *Front. Physiol.* **2021**, *12*. [CrossRef]
10. Lightner, D.J.; Gomelsky, A.; Souter, L.; Vasavada, S.P. Diagnosis and Treatment of Overactive Bladder (Non-Neurogenic) in Adults: Aua/Sufu Guideline Amendment 2019. *J. Urol.* **2019**, *202*, 558–563. [CrossRef]
11. Norderval, S.; Rydningen, M.; Lindsetmo, R.-O.; Lein, D.; Vonen, B. Sacral nerve stimulation. *Tidsskr. Nor. Legefore.* **2011**, *131*, 1190–1193. [CrossRef] [PubMed]
12. Siegel, S.W.; Catanzaro, F.; Dijkema, H.E.; Elhilali, M.M.; Fowler, C.J.; Gajewski, J.B.; Hassouna, M.M.; Janknegt, R.A.; Jonas, U.; Van Kerrebroeck, P.E. Long-term results of a multicenter study on sacral nerve stimulation for treatment of urinary urge incontinence, urgency-frequency, and retention. *Urology* **2000**, *56*, 87–91. [CrossRef]
13. Jonas, U.; Fowler, C.; Chancellor, M.; Elhilali, M.; Fall, M.; Gajewski, J.; Grünewald, V.; Hassouna, M.; Hombergh, U.; Janknegt, R. Efficacy of sacral nerve stimulation for urinary retention: Results 18 months after implantation. *J. Urol.* **2001**, *165*, 15–19. [CrossRef] [PubMed]
14. Brazzelli, M.; Murray, A.; Fraser, C. Efficacy and safety of sacral nerve stimulation for urinary urge incontinence: A systematic review. *J. Urol.* **2006**, *175*, 835–841. [CrossRef]
15. Peters, K.M.; Carrico, D.J.; Wooldridge, L.S.; Miller, C.J.; MacDiarmid, S.A. Percutaneous tibial nerve stimulation for the long-term treatment of overactive bladder: 3-year results of the STEP study. *J. Urol.* **2013**, *189*, 2194–2201. [CrossRef]
16. Slovak, M.; Chapple, C.R.; Barker, A.T. Non-invasive transcutaneous electrical stimulation in the treatment of overactive bladder. *Asian J. Urol.* **2015**, *2*, 92–101. [CrossRef]
17. Seth, J.H.; Gonzales, G.; Haslam, C.; Pakzad, M.; Vashisht, A.; Sahai, A.; Knowles, C.; Tucker, A.; Panicker, J. Feasibility of using a novel non-invasive ambulatory tibial nerve stimulation device for the home-based treatment of overactive bladder symptoms. *Transl. Androl. Urol.* **2018**, *7*, 912. [CrossRef]
18. Lee, J.; Park, E.; Kang, W.; Kim, Y.; Lee, K.-S.; Park, S.-M. An efficient noninvasive neuromodulation modality for overactive bladder using time interfering current method. *IEEE Trans. Biomed. Eng.* **2020**, *68*, 214–224. [CrossRef]
19. Yang, C.; Park, S. Nanomaterials-assisted thermally induced neuromodulation. *Biomed. Eng. Lett.* **2021**, *11*, 163–170. [CrossRef] [PubMed]
20. Grossman, N.; Bono, D.; Dedic, N.; Kodandaramaiah, S.B.; Rudenko, A.; Suk, H.-J.; Cassara, A.M.; Neufeld, E.; Kuster, N.; Tsai, L.-H. Noninvasive deep brain stimulation via temporally interfering electric fields. *Cell* **2017**, *169*, 1029–1041.e16. [CrossRef]

21. Bai, S.; Dokos, S.; Ho, K.-A.; Loo, C. A computational modelling study of transcranial direct current stimulation montages used in depression. *Neuroimage* **2014**, *87*, 332–344. [CrossRef]

22. Kilgore, K.L.; Bhadra, N. Reversible nerve conduction block using kilohertz frequency alternating current. *Neuromodulation: Technol. Neural Interface* **2014**, *17*, 242–255. [CrossRef]

23. Lee, S.; Lee, C.; Park, J.; Im, C.-H. Individually customized transcranial temporal interference stimulation for focused modulation of deep brain structures: A simulation study with different head models. *Sci. Rep.* **2020**, *10*, 1–11. [CrossRef]

24. Miranda, P.C.; Mekonnen, A.; Salvador, R.; Ruffini, G. The electric field in the cortex during transcranial current stimulation. *Neuroimage* **2013**, *70*, 48–58. [CrossRef] [PubMed]

25. Saturnino, G.B.; Madsen, K.H.; Siebner, H.R.; Thielscher, A. How to target inter-regional phase synchronization with dual-site transcranial alternating current stimulation. *Neuroimage* **2017**, *163*, 68–80. [CrossRef]

26. Cao, J.; Grover, P. Stimulus: Noninvasive dynamic patterns of neurostimulation using spatio-temporal interference. *IEEE Trans. Biomed. Eng.* **2019**, *67*, 726–737. [CrossRef] [PubMed]

27. Xin, Z.; Kuwahata, A.; Liu, S.; Sekino, M. Magnetically induced temporal interference for focal and deep-brain stimulation. *Front. Hum. Neurosci.* **2021**, *15*, 693207. [CrossRef]

28. Lee, S.; Park, J.; Lee, C.; Im, C.-H. Multipair transcranial temporal interference stimulation for improved focalized stimulation of deep brain regions: A simulation study. *Comput. Biol. Med.* **2022**, *143*, 105337. [CrossRef] [PubMed]

29. Huang, Y.; Parra, L.C. Can transcranial electric stimulation with multiple electrodes reach deep targets? *Brain Stimul.* **2019**, *12*, 30–40. [CrossRef] [PubMed]

30. Li, W. Biomechanics of infarcted left ventricle: A review of modelling. *Biomed. Eng. Lett.* **2020**, *10*, 387–417. [CrossRef]

31. Gabriel, C. *Compilation of the Dielectric Properties of Body Tissues at RF and Microwave Frequencies*; King's College London (United Kingdom) Department of Physics: London, UK, 1996.

32. Reato, D.; Rahman, A.; Bikson, M.; Parra, L.C. Low-intensity electrical stimulation affects network dynamics by modulating population rate and spike timing. *J. Neurosci.* **2010**, *30*, 15067–15079. [CrossRef] [PubMed]

33. Hsu, W.-Y.; Zanto, T.P.; Gazzaley, A. Parametric effects of transcranial alternating current stimulation on multitasking performance. *Brain Stimul.* **2019**, *12*, 73–83. [CrossRef] [PubMed]